 ICCES, vol.4, no.1, pp.11-18, 2007

Incompressible Viscous Flow Simulations Using the Petrov-Galerkin Finite Element Method

Kazuhiko Kakuda[1], Tomohiro Aiso[1] and Shinichiro Miura[2]

Summary

The applications of a finite element scheme to three-dimensional incompressible viscous fluid flows are presented. The scheme is based on the Petrov-Galerkin weak formulation with exponential weighting functions. The incompressible Navier-Stokes equations are numerically integrated in time by using a fractional step strategy with second-order accurate Adams-Bashforth scheme for both advection and diffusion terms. Numerical solutions for flow around a circular cylinder and flow around a railway vehicle in a tunnel are presented.

Introduction

From the computational point of view, the numerical simulations of three-dimensional viscous fluid flows up to high Reynolds number are indispensable in science and engineering fields. Numerical instabilities have been experienced in the solution of incompressible Navier-Stokes equations at a high Reynolds number. To stabilize such calculations, various upwind schemes have been successfully presented in finite difference and finite element frameworks [1,2].

We have developed a finite element scheme based on the Petrov-Galerkin weak formulation using exponential weighting functions for solving accurately and in a stable manner the flow field of an incompressible viscous fluid up to high Reynolds number regimes [3,4]. The Navier-Stokes equations are semi-explicitly integrated in time by using a fractional step strategy, and hence split into the advection-diffusion eqution and linear Euler-type equtions. As the time-marching scheme, we adopt effectively the second-order accurate Adams-Bashforth explicit differencing for both advection and diffusion terms.

The purpose of this paper is to present the application of the Petrov-Galerkin finite element scheme using exponential weighting functions to various flow problems in three-dimensional incompressible viscous fluid. The workability and validity of the present approach are demonstrated through flow around a circular cylinder [5-10] and flow around a railway vehicle in a tunnel up to high Reynolds number.

Statement of the Problem

The motion of an incompressible viscous fluid flow is governed by the Navier-Stokes equations in dimensionless form. By applying the time splitting technique

[1]Department of Mathematical Information Engineering, College of Industrial Technology, Nihon University, Chiba 275-8575, Japan E-mail:k7kakuda@cit.nihon-u.ac.jp

[2]Department of Mechanical Engineering, Tokyo Metropolitan College of Technology, Tokyo 140-0011, Japan

to the set of equations, we can split formally the problem into the following two parts :

$$\dot{u}_i(\tilde{u}_i, u_i^n) + u_j u_{i,j} = \frac{1}{Re} u_{i,jj} \qquad in\ \Im \times \Omega \tag{1}$$

$$\dot{u}_i(u_i^{n+1}, \tilde{u}_i) = -p_{,i}\ ,\ u_{i,i} = 0 \qquad in\ \Im \times \Omega \tag{2}$$

In these expressions, u_i is the velocity vector component, p is the pressure, Re is the Reynolds number, $\tilde{u}_i$ is the auxiliary velocity vector, and u_i^n denotes the value of u_i at time level $n\Delta t$, where Δt is a time increment.

Petrov-Galerkin Finite Element Formulation

Let us now consider the Petrov-Galerkin finite element formulation using exponential weighting functions [4] to equation (1). By applying the divergence theorem to the weighted residual form of equation (1), and after some manipulations, we have the following weak form :

$$\int_{\Omega_e} \left\{ \dot{u}_i(\tilde{u}_i, u_i^n) + u_j u_{i,j} \right\} M_\alpha d\Omega + \int_{\Omega_e} \frac{1}{Re} u_{i,j} N_{\alpha,j} d\Omega = \int_{\Gamma_e} \tau_i N_\alpha d\Gamma \tag{3}$$

where $\tau_i \equiv u_{i,j} n_j / Re$, Ω_e is a subdomain of the whole domain Ω, Γ_e is the boundary on the subdomain, and M_α denotes the weighting function given by

$$\left.\begin{aligned} M_\alpha(x) &= \sum_{\gamma,i} N_\alpha(x) e^{-a_i(N_\gamma x_i^\gamma - x_i^\alpha)} \\ a_i &= \frac{\alpha_i}{|L_i|} sgn(v_i) \end{aligned}\right\} \tag{4}$$

where N_α is the shape function in three dimensions, v_i is the velocity vector averaged in Ω_e, L_i is the reference length for x_i-directions, α_i is the upwinding parameters which control an effect of the upwinding, and $sgn(v_i)$ denotes the signum function.

At this stage, by using the second-order accurate Adams-Bashforth strategy as a time integration scheme, we have the finite element system of equations [4]. On the other hand, the conventional Galerkin finite element formulation can be applied to solve numerically the set of equation (2).

Numerical Examples

In this section we present numerical results obtained from applications of the above-mentioned numerical method to incompressible viscous flow problems. In our numerical performances, we adopt the lowest interpolation functions in which the velocity and the scalar potential are piecewise trilinear, and the pressure is constant over each element. The initial velocities are assumed to be zero everywhere in the interior domain.

Flow around a circular cylinder

We shall consider the flow around a circular cylinder. Fig.1 shows the geometry with the boundary conditions, the finite element mesh, and the configuration of the closed wake of the flow around a circular cylinder. The Reynolds number,Re, based on the uniform velocity,U_0, at the inflow and the diameter,D, of the cylinder is up to 10^6. The parameters that characterize the finite element approximation are summarized in Table 1. Fig.2 shows the streamlines and pressure fields at early times around the cylinder in horizontal x_1x_2-section at $x_3 = 2.0$ for different Reynolds numbers up to 9500. The quantitative comparisons of the main wake length and the twin vortex characteristics behind the cylinder are shown in Fig.3. For the Reynolds numbers of 550 and 3000 our numerical results are in good agreement with the experimental data [5] and other numerical data [6,7]. For $Re = 9500$ our predictions of the main wake length are slightly defferent to the experimental data [5], while the present results are similar to the other numerical data [6]. Fig.4 shows the instantaneous streamlines and pressure fields around the cylinder in the horizontal center cross-section for different high Reynolds numbers. From these results, it is interesting that the separation points on the cylinder shift on the leeward at $Re = 5 \times 10^5$. As a result, it is clear that the width of the wake is considerably narrower than those up to subcritical Reynolds number of 10^5. In Fig.5, we give the time-averaged pressure distributions along the surface of the cylinder for several Reynolds numbers, and also compare with the experimental data [8,9]. The peak magnitudes of our profile at $Re = 10^5$ seem to be overestimated conspicuously in comparison with the experimental data [8], while the agreement between the present and the peak magnitudes of other experimental data using a short cylinder appears satisfactory. At $Re = 5 \times 10^5$, the present results are in good agreement with the experimental data [9]. In Fig.6 we give the time-averaged drag coefficient, $\overline{C}_d$, and the Strouhal number, S_t, through comparison with experimental data [8] and other numerical solutions [2,10]. The minimum value of the present drag coefficients is 0.4572 at $Re = 5 \times 10^5$. The correlation between the present results and some other data appears satisfactory except the solutions of 2D flow simulations up to Reynolds number of 10^4. The present results for the Strouhal number are also qualitatively similar to the experimental data.

Table 1: A summary of the parameters

Re	Nodes	Elements	l_{min}	$\triangle t$	α_i
550	179,970	168,000	0.00341	0.001	0.2
3000	179,970	168,000	0.00341	0.002	0.4
9500	179,970	168,000	0.00341	0.002	0.4
10^4	179,970	168,000	0.00341	0.002	0.4
$10^5 - 10^6$	179,970	168,000	0.00341	0.002	1.0

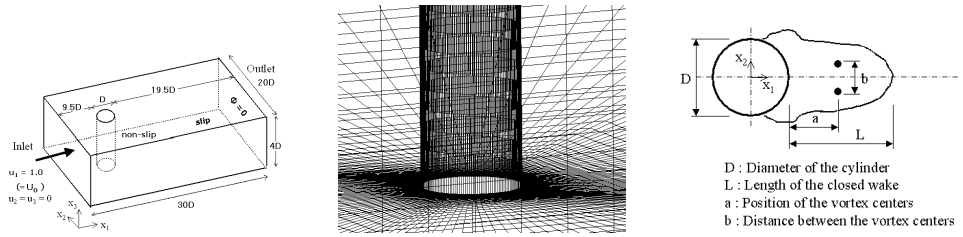

(a) Geometry and boundary conditions (b) Finite element mesh (c) Configuration of the closed wake

Figure 1: Flow around a circular cylinder

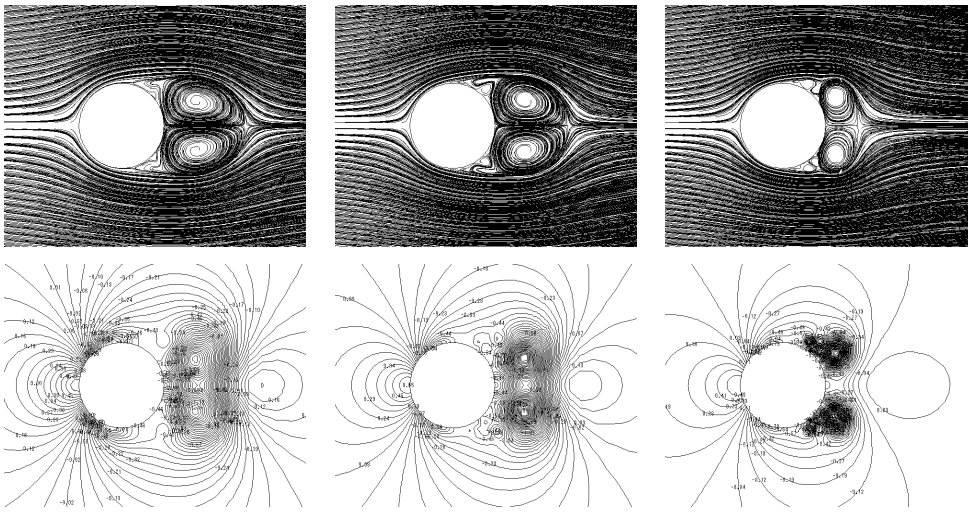

(a) $Re = 550$ (b) $Re = 3000$ (c) $Re = 9500$

Figure 2: Streamlines and pressure fields

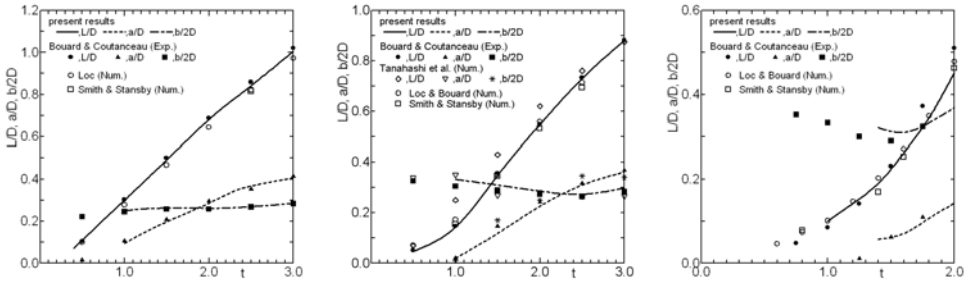

(a) $Re = 550$ (b) $Re = 3000$ (c) $Re = 9500$

Figure 3: Main-wake length and the characteristics of a twin vortex

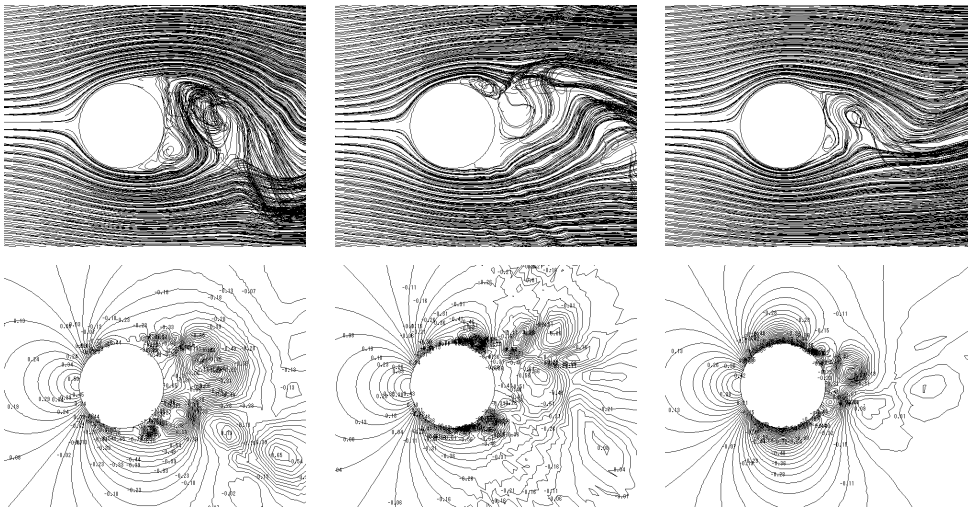

(a) $Re = 10^4$ (b) $Re = 10^5$ (c) $Re = 5 \times 10^5$

Figure 4: Streamlines and pressure fields

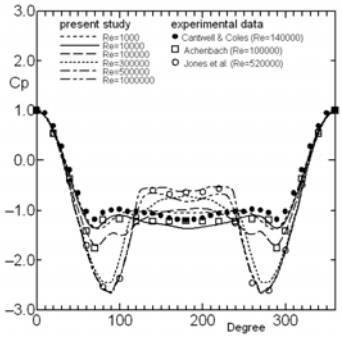

Figure 5: Time-averaged pressure distributions

Flow around a railway vehicle in a tunnel

As the second example, we shall consider the flow around a railway vehicle for different shapes. Fig.7 shows the geometry, the boundary conditions, and the finite element mesh of the flow around a railway vehicle. The Reynolds numbers, Re, based on the uniform velocity, U_0, at the inflow and the diameter of the wheel, D, are 10^5 and 10^6, respectively. The parameters that characterize the finite element approximation are summarized in Table 2. Fig.8 shows the instantaneous streamlines around rear and side surfaces of the railway vehicle for $Re = 10^5$ and 10^6. The corresponding pressure fields are shown in Fig.9. From the streamlines at $Re = 10^6$(see Fig.8(b)), there appears to have the flow behavior in x_1-direction

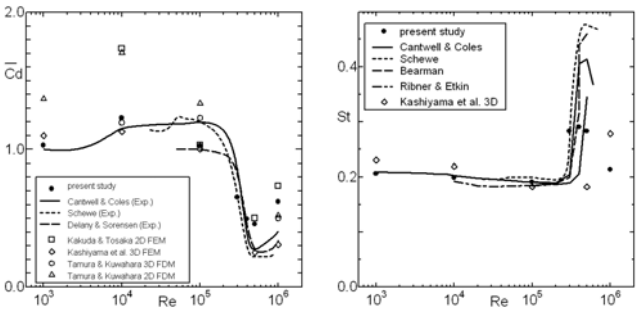

(a) Drag coefficients (b) Strouhal numbers

Figure 6: Time-averaged drag coefficients and Strouhal numbers

behind the railway and the longitudinal vortices are appeared in the downstream region of the railway vihicle.It is also clear from the pressure field(see Fig.9(b)). In Fig.10 we give the distributions of Powell's sound source term, $\nabla \cdot (\omega \times u)$. Here, Powell's sound source term is a value acquired from the right-hand side of Powell equation, $\partial^2 \rho / \partial t^2 - a_0^2 \nabla^2 \rho = \rho_0 \nabla \cdot (\omega \times u)$. It turns out that the noises occur mainly near the front and top-edge regions of the railway vehicle.

Table 2: A summary of the parameters

Case	Nodes	Elements	l_{min}	Δt	α_i
1	368,760	310,940	0.024	0.01	0.25
2	453,442	386,040	0.024	0.01	0.25

(a) Geometry and boundary conditions (b) Finite element mesh(Case 2)

Figure 7: Flow around a railway vehicle in a tunnel

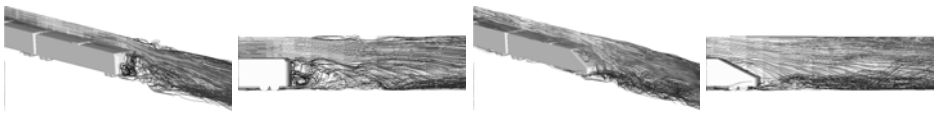

(a) $Re = 10^5$ (Case 1) (b) $Re = 10^6$ (Case 2)

Figure 8: Instantaneous streamlines

Conclusions

We have presented a finite element scheme for solving numerically three-dimen-

(a) $Re = 10^5$ (Case 1) (b) $Re = 10^6$ (Case 2)

Figure 9: Instantaneous pressure fields

(a) $Re = 10^5$ (Case 1) (b) $Re = 10^6$ (Case 2)

Figure 10: Distribution of sound sources

sional incompressible Navier-Stokes equations. The scheme is based on the Petrov-Galerkin finite element formulation using exponential weighting functions. The set of equations is numerically integrated in time by using the second-order accurate Adams-Bashforth strategy for both advection and diffusion terms.

As the numerical examples, flow around a circular cylinder and flow around a railway vehicle in a tunnel are simulated up to high Reynolds number regimes. The numerical results for flow around a circular cylinder are qualitatively and quantitatively in good agreement with experimental data and other numerical ones. The numerical results also demonstrate that the present approach is capable of solving three-dimensional incompressible Navier-Stokes equations in a stable manner up to high Reynolds numbers.

References

1. Brooks, A. and Hughes, T.J.R. (1982): "Streamline Upwind / Petrov-Galerkin Formulations for Convection Dominated Flow with Particular Emphasis on the Incompressible Navier-Stokes Equations", *Comp. Meths. Appl. Mech. Engng.*, **32**, pp.199-259.
2. Tamura, T. and Kuwahara, K. (1989): "Direct Finite Difference Computation of Turbulent Flow around a Circular Cylinder", *Num. Meths. Fluid Dyns. U*, (Eds., M. Yasuhara *et al.*), pp.645-650.
3. Kakuda, K. and Tosaka, N. (1992): "Finite Element Approach for High Reynolds Number Flows", *Theoretical and Applied Mechanics*, **41**, pp.223-232.
4. Kakuda, K. (2004): "Finite Element Computations of Flow around a Wall-Mounted Cube", *Int. J. Comp. Fluid Dyns.* **18**(5), pp.393-399.
5. Bouard, R. and Coutanceau, M. (1980): "The Early Stage of Development

of the Wake behind an Impulsively Started Cylinder for $40 < Re < 10^4$", *J. Fluid Mech.* **101**, part 3, pp.583-607.

6. Ta Phuoc Loc and Bouard, R. (1985): "Numerical Solution of the Early Stage of the Unsteady Viscous Flow around a Circular Cylinder: A Comparison with Experimental Visualization and Measurements", *J. Fluid Mech.* **160**, pp.93-117.
7. Tanahashi, T., Okanaga, H. and Saito, T. (1990): "GSMAC Finite Element Method for Unsteady Incompressible Navier-Stokes Equations at High Reynolds Numbers", *Int. J. Num. Meth. Fluids*, **11**, pp.479-499.
8. Cantwell, B. and Coles, D. (1983): "A Experimental Study of Entrainment and Transport in the Turbulent near Wake of a Circular Cylinder", *J. Fluid Mech.* **136**, pp.321-374.
9. Jones, G.W., Cincotta, J.J. and Walker, R.W. (1969): "Aerodynamic Forces on a Stationary and Oscillating Circular Cylinder at High Reynolds Numbers", *NASA TR* R-300.
10. Kashiyama, K., Tamai, T., Inomata, W. and Yamaguchi, S. (1998): "A Parallel Finite Element Method for Incompressible Navier-Stokes Flows Based on Unstructured Grid", *4th Japan-US Symp. F.E.M. in Large-Scale Computational Fluid Dynamics*, pp.21-24.
11. Powell, A. (1964): "Theory of Vortex Sound", *J. Acoust. Soc. Am.*, **36**, pp.177-195.